LYCEN 9347
September 1993

Secondary ion emission from ultra-thin oxide layers bombarded by energetic (MeV) heavy ions : depth of origin and layer homogeneity

H. Allali[1] B. Cabaud[2], G. Fuchs[2], A. Hoareau[2], B. Nsouli[1], J-P. Thomas[1], M. Treilleux[2] and J.S. Danel[3]

[1]Institut de Physique Nucléaire de Lyon, IN2P3-CNRS/Univ. Claude Bernard
43, Bd du 11 Novembre 1918, F-69622 Villeurbanne cedex, France

[2]Département de Physique des Matériaux, Univ. Claude Bernard Lyon I, 43 Boulevard du 11 Novembre 1918, 69622 Villeurbanne Cedex, France

[3]LETI/DOPT/SCMM, Commissariat à l'Energie Atomique, Centre d'Etudes Nucleaires de Grenoble, 85X-38041 Grenoble Cedex, France

Abstract

The escape depth of the secondary ions resulting from electronic sputtering of fast heavy ions in inorganic thin films has been investigated. Chromium layers deposited onto SiO_2 substrate as well as SiO_x layers deposited onto chromium substrate have been characterised by secondary ion emission mass spectrometry (SIMS) in combination with time-of-flight (TOF) mass analysis (also referred as HSF-SIMS [1]). These crossed experiments lead to a value around 1 nm for SiO_x layers and 0.5 nm for Cr layers. On the other hand, HSF-SIMS can be used to correlate the intensity of the secondary ion emission to the film coverage rate (Θ) and (or) the morphology of particular films like those produced by Low Energy Cluster Beam Deposition (LECBD). Using Sb deposits, the non-linear relationship between ion emission and Θ is interpreted in terms of sputtering enhancement in the individual supported clusters.

To be published in NIM B

1. Introduction

The depth of origin of sputtered particles has been for long a subject of debate in low-velocity ion-impact SIMS (LSF-SIMS [1]) because of the not fully convincing results from a limited number of experimental data (see for example ref [2]). When most of the theoretical predictions ascribe more than 80 % of the emission to the top monolayer, the experimental problem lies on the obtention of ultra-thin layers for which there is an unambiguous relationship between thickness and coverage. The best results to date have been for metals or semiconductors. However, in the case of HSF-SIMS, based on electronic sputtering, the material must be dielectric. In that respect, the essential of the investigations to date has been obtained from molecular organic films [3, 4] prepared by the Langmuir-Blodgett (LB) technique [5].

Such a technique is almost ideal since the films are built onto a metallic substrate monolayer by monolayer (identical or different), the knowledge of the molecular area and the molecule length, defining the thickness. Then, one of the most accepted feature for HSF-SIMS is the increase of the molecular ion yield with the thickness up to a saturation limit at approximately 6-8 monolayers (15-20 nm), with some evidence for a volume emission [6]. (Here and in the following, the experimental emission yield is the number of given secondary ions per primary ion). In sharp contrast to these findings, a very unlike situation has been reported by R. Macfarlane et al [7] showing that for evaporated deposits of Cs salts onto polypropylene as well as Rhodamine 6-G hydrochloride, the secondary ion yield reached saturation at one monolayer coverage. To our knowledge, nothing has been reported concerning any other deposits.

There are several reasons for selecting oxide films to investigate the depth of emission in the case of inorganics. Among them, silicon oxide is a very good candidate as far as thin and homogeneous evaporated layers are concerned since they are known for having high fixing properties especially to protect very thin layers deposited under vacuum from air transfer [8, 9]. On the other hand, oxide films have not necessarily to be prepared from that chemical form. As it will be demonstrated in the following, secondary ion emission can be induced in

metallic films from their native oxide which develops more or less rapidly. However, due to the original metallic character, a good correlation between resistivity and homogeneity can be obtained during the growing of such films onto insulator substrates. Then, chromium is particularly interesting because it exhibits good wetting properties on insulating surfaces, and the conductivity of the film starts to increase from thickness values as low as 0.2 nm [10]. More recently, experimental depth-profiling of a one monolayer thick chromium deposit has also been reported [11].

From these particular materials, uniform layers of low thickness are expected, but one must be cautious about the morphology of the first growth stage where 3-dimensional islands are formed as a consequence of the high interfacial energy between the film and the substrate(see for example ref. [12]). Low-energy cluster beam deposition (LECBD) represents an alternative to this general trend since the growth of such films proceeds from a "two-dimensional mechanism" (paving of the substrate by incident clusters) [13]. Then, metallic supported clusters films can grow, and, among others, antimony is a good candidate for reproducible films with a well controlled morphology on various materials [13, 14]. To emphasise this feature, it is worth pointing out the definite advantage of Sb films made from LECBD over those resulting from classical molecular beam deposition (MBD): with an electric percolation threshold decreasing from 37 nm for MBD to 2.2 nm for LECBD, there is a one order of magnitude gain in the equivalent thickness range of continuous films [15]. For such a well documented growth behaviour, one may then expect either to correlate the variation of the characteristic ion yield variation to the coverage or to the morphology (grain size effect).

In the present paper we demonstrate that negative secondary ion emission induced in such films by high energy (9 MeV) Ar ion bombardment is not only a valuable tool for the determination of the escape depth of these secondary ions but can also be related to the morphology of the film. In addition, the characteristic emission of the layer or (and) of the substrate often consists of polyanion clusters of various masses. Their respective yield variation as a function of the layer thickness or composition give also an insight in the emission process.

2. Experimental

Chromium films are vacuum evaporated (electron gun bombardment) from a crucible located 21 cm from the rotating (40 rot./mn) substrate holder. The temperature is maintained at 150° C during evaporation. The deposition rate has to be set between 3. 10^{-2} nm/s and 0.3 nm/s depending of the required thickness. This last parameter is adjusted from the indications of a piezo-electric system, which has been calibrated using various techniques. Among them, ESCA measurements have been performed for the thinnest layers taking advantage of the 1.25 nm value of the inelastic mean free path of the Cr(2p) photoelectrons [11]. We have systematically checked the quoted values by performing 3 MeV α-particles RBS at 150°. As illustrated by the spectrum represented in fig.1, the sensitivity is pretty high, and the absolute precision does not exceed 10%. Accordingly, the values of equivalent linear thickness reported in table 1 can be considered as in excellent agreement with the expectations. Finally, the TEM photograph taken from a 1nm thick layer and represented in fig.2, is indicative of an almost complete coverage.

The deposition of SiO_X films from a Knudsen cell loaded with silicon monoxide powder was performed on various susbtrates located 20 cm away (Thick films of Cr and Sb, crystal of CsI) in a vacuum chamber pumped to below 10^{-4} Pa. The deposition rate, monitored directly by a quartz crystal oscillator, was fixed a 0.03 nm/s .The thickness range lay between 0.5 and 20 nm, values also ascertained by RBS measurements but from films deposited onto carbon substrates.

The Sb clusters used to grow LECBD films are generated by the gas aggregation technique in a source similar to the one developed by Sattler [16]. The metallic vapour coming from a heated crucible condenses in an inert gas (argon in the present case) cooled at liquid nitrogen temperature. The cluster size, monitored by the argon pressure, has a distribution which is measured by a time-of-flight mass spectrometer [17]: a mean size of 1300 atoms has been determined, which corresponds to a mean cluster diameter of 4.5 nm (assuming a spherical shape and a bulk density for Sb free clusters). The neutral clusters are deposited on substrates of different nature (Si wafers, a-C films, ...) at room temperature with a rate around

5×10^{-3} nm s^{-1} (corresponding to a cluster flux typically of 10^{10} clusters cm^{-2} s^{-1}). The thickness, ranging from 1 to 30 nm, is controlled by a crystal quartz rate monitor located near the substrates. Absolute calibration has also been checked using MeV helium ion Rutherford Backscattering (RBS).

In the low thickness range, it is of prime importance to relate the thickness value to the coverage rate Θ of the film. The evolution of Θ versus thickness has been determined by transmission electron microscopy (TEM). TEM observations have been carried out using a 200-CX Jeol electron microscope operating at 200 kV accelerating voltage. Of course, since our deposition conditions do not fulfil ultra-high-vacuum (UHV) standards, checks have been made to ensure that the nature of the substrate is not critical in the measurements of the coverage rate.

Argon ions in the MeV range are convenient projectiles for inducing electron and ion emission in the target of interest from the 4 MV Van De Graaff accelerator of the Institut de Physique Nucléaire de Lyon [18]. We use typically triply charged ions around 9 MeV since the electronic stopping power is at about 80% of its maximum value, at which most secondary ion yields reach their maximum. The intensity of the beam as well as its size are kept respectively to several hundred projectiles per second and to several tenths of millimetere by using a fixed collimator at the upstream beam focal point and crossed slits of adjustable width 80 cm from the target. An upper limit of the spot size has been estimated to be 0.12 mm .

As reported in a recent paper [19], our TOF system 12.5 cm long, has been designed for a 100% transmission through the use of a focusing electrode located 2.5 cm from the target. It is schematically represented in fig.3. When thick targets are concerned, TOF measurements cannot be performed using as start signals those resulting from the detection in a surface barrier detector (SBD) of the primary ions transmitted through these targets. However, for negative ions, one can take advantage of the fact that each impact leads to the emission of an electron shower with a 100% detection efficiency. On the other hand, these electrons will always reach the multi-channel plate (MCP) detector of the secondaries first. Then, once splitted, the same signal can be used for the generation of the start signal, triggering its delayed counterpart where the stop signals are taken from the same event of electrons followed by

negative ions. Such start and stop signals are processed by a time-digital converter (TDC). In this particular experiment, ejected secondary ions and electrons are extracted and accelerated by a potential difference of 5 kV between the biased target and a grounded stainless steel annular electrode with an internal diameter of 5 mm. This simple technique is often described as "start electron". Electronics units used for this processing are also sketched in fig 3.

Typical spectra obtained under these experimental conditions are represented in fig 4, for chromium deposited onto a quartz substrate and for its mirror system SiO_x deposited onto a chromium layer. It can be seen that the peaks taken from the bare quartz substrate (Fig. 4a) correspond to masses 63 and 79, respectively atttributed to $SiO_2H_3^-$ and $Si(OH)_3^-$: they are characterisic of silicon oxide surfaces exposed to air [20]. For a 1 nm thick chromium layer (Fig. 4b), the previous peaks have almost disappeared, while the new peaks corresponding to the presence of chromium are for masses 85, 101 and 169, respectively atttributed to the oxyanions CrO_2H^-, CrO_3H^- and $Cr_2O_4H^-$. As for silicon, polyatomic ions characteristic of chromium oxide layers resulting from air exposure incorporate hydrogen. On the other hand, these peaks can be observed from the emission of a chromium substrate through a SiO_x layer 0.5 nm thick (Fig. 4c), on top of it. It can be observed that the emission of the peaks corresponding to masses 63 and 79 is weaker than for the quartz case, but sufficient to attest for the presence of the SiO_x layer 1 nm thick together with the vanishing of the Cr oxyanions (Fig. 4d).

The secondary ion emission for a Sb layer consists of the oxyanion clusters $[(SbO_2)_n]^-$ and $[(SbO_2)_nSbO]^-$ respectively labelled A_n and B_n on the spectra of fig 5, from which SbO_2^-, $Sb_2O_4^-$ and $Sb_3O_5^-$ exhibit the most intense emission. For such a layer 1.6 nm thick, the coverage is below 50% and consequently secondary ion emission from the silicon substrate should be observed. Indeed, the mass 79 is observed on fig 5, but not the mass 63. In addition, such a peak is also observed with much thicker layer and the existence of a contaminant is then highly suspected. Finally, it has been shown that the oxyanion emission is evolving with air exposure [21], but the observed kinematics does not affect our comparative measurements between samples of different thickness.

3. Results

3.1. The Silicon oxide-chromium system.

We have represented in fig.6a, the variation of the yield of the ions CrO_2H^- and CrO_3H^- as a function of the chromium layer thickness. The respective values being accidentally close, no normalisation was required and the error bars on the data account for a sampling of two targets taken from the same deposit. It can be seen that, at 0.5 nm, the chromium yield is about 90% of the saturation value in very good agreement with the 90% reduction of the $Si(OH)_3^-$ yield, characteristic of the quartz substrate.

The variation of the yield of $Si(OH)_3^-$ as a function of the SiO_x layer thickness results from two sets of experiments which have been separetely performed on two sets of deposits of increasing thickness :1, 2 and 20 nm for the first batch, 0.5, 1, 6, 10 and 20 nm for the second, both onto a chromium thick layer (10 nm) backing. The corresponding data are represented in fig. 6b, showing a definite $Si(OH)_3^-$ yield saturation at 1 nm. Matching this variation, the $CrOH_3^-$ ion yield is continuously decreasing down to a zero value.

For such a 1 nm thickness, an identical value of the $Si(OH)_3^-$ yield is found when the layer is deposited onto a thick (30 nm) Sb layer backing. As for the previous case, the ion emission from the substrate is also undetectable. For a smaller thickness (0.5 nm in the present case), the yield reduction from the value corresponding to the uncovered substrate can be different for different substrates as shown in fig. 7. Assuming an identical SiO_x coverage for the three substrates, it appears that the yield reduction is systematically higher for the polyatomic ion of the lowest mass, as shown in the insert of fig. 7. Such a result, if confirmed on a larger thickness range, could be important for the understanding of the origin of cluster formation within a layer.

To sum up, the system silicon oxide-chromium appears to be a very favorable one, since there is a mirror variation of the yield of the ions coming respectively from the layer and from the substrate, as a function of the layer thickness. Moreover, this is also observed from the symmetric system, both experiments leading to a depth of origin value between 0.5 and 1 nm or "one and two monolayers".

3.2. LECBD antimony layers.

To extract more information about the basic mechanism of HSF-SIMS, we have studied the variation of the emission yield Y as function of the coverage rate Θ of the analysed surface. For LECBD antimony layers, the variation of Θ versus thickness is well controlled and low compared to the chromium-silicon oxide for which Θ reaches 100% for a 1 nm Cr thick-film. For these two reasons, LECBD antimony layers appear to be a favourable choice to characterise the emission yield evolution versus Θ.

The evolution of the coverage rate Θ as a function of the average film thickness is represented in fig 8. The experimental results (curve c) are compared with two simple models :

- the random staking of incident clusters (curve a) is a correct description of the experimental results in the low thickness range.

- when the thickness increases, overlapping events have to be considered: this leads to the theoretical curve (b), which is a fair approximation of the experimental curve.

The knowledge of the relationship between the equivalent thickness and Θ allows us to plot in fig 9 the variation of the yield of the ions SbO_2^- and $Sb_2O_4^-$ as a function of Θ. As a first approximation, it is reasonable to expect a linear dependence between the ion yield and the developed surface of the film, which should vary as the coverage rate. As a matter of fact, the growing of LECBD Sb films proceeds from a paving of the substrate by incident clusters, which maintain their integrity when the overlapping proceeds. Such a linear variation of the ion yields between 0 and 100 % of the coverage rate is not observed: following a fast increase at low values, the saturation is almost achieved at the percolation threshold (apparent depth of 3.3 nm, slightly below the mean diameter-4 nm- of the cluster). It should be noted that the experimental data points are from two independent batchs, one corresponding to the values 3, 15, 38 and 54 %, the other for 38, 78 and 100 %. With such a large discrepancy with an expected linear increase , one cannot exclude at low coverage, an enhancement of the emission yield when a large fraction of the energy of the incoming ion has to be dissipated in the small volume of the supported cluster (4.5 nm diameter). Such a grain size effect has already been reported for fission fragments interacting with various materials, metal or oxides [22].

Of course, it would have been of great help to look simultaneously at the emission signal of the substrate, as it was progressively covered. Taking silicon as a substrate was dictated by our well documented study of the film morphology but the most intense secondary emission is for mass 79, which is a strong contaminant of the Sb layers. Additionnal experiments are in progress to obtain a more detailed experimental curve should include data from the substrate, for which correlation between thickness and coverage should to be confirmed.

4. Conclusion

From the secondary ion emission of both deposited layers and underneath substrate, one can estimate the depth of origin of ions resulting from electronic sputtering. From evaporated layers of chromium of increasing thickness onto a quartz substrate, it is shown that around 0.5 nm, there is a saturation in the emission yield characteristic of the layer corresponding to an extinction of those of the substrate. From evaporated layers of silicon oxide, SiOx, onto a chromium backing, the corresponding value appears to be 1 nm. This last result has been reproduced for three different substrates. Such a value corresponds to about 2 monolayers, which is strikingly different from the commonly reported value of 8 - 10 monolayers for organic materials layers.

In the particular case of antimony cluster beam deposition, a relationship between average thickness of the layer and coverage rate has been established, in agreement with a random stacking growth of the layer. The variation of the secondary ion emission yield as a function of the coverage rate is only qualitatively in agreement with this growing mechanism. There are indications either of a complex morphology or of an enhanced emission from the low coverage material or both.

Well characterized ultra-thin layers will undoubtly lead to more precise determinatoion of depth of origin of secondary ions. Conversely, the use of HSF-SIMS for investigating growing mechanisms appears to be very important together with surface techniques.

Acknowledgements:

Dedicated assistance of the accelerator crew, M. Ferrari, A. Gardon and C. Devesa, as well as support from B. Lagrange and M. Lambert are greatly acknowledged.

References:

[1] B.U.R. Sundqvist in "Sputtering by Particle Bombardment III" ed. by R. Behrisch and K. Wittmaack (Springer-Verlag Berlin Heidelberg 1991) p. 257

[2] K. Wittmaack in "Sputtering by Particle Bombardment III" ed. by R. Behrisch and K. Wittmaack (Springer-Verlag Berlin Heidelberg 1991) p. 169

[3] G. Säve, P. Hakansson, B.U.R. Sundqvist, E. Söderström, S.-E. Lundquist and J. Berg, Int. J. of Mass Spec. and Ion Proc., 78, (1987), 259

[4] G. Bolbach, A. Viari, R. Galera, A. Brunot and J.C. Blais, Int. J. of Mass Spec. and Ion Proc., 112, (1992), 93

[5] V. K. Agarwal, Phys. Today, (1988) 40

[6] S. Della Negra, J. Depauw, H. Joret, Y. Le Beyec , I.S. Bitensky, G. Bolbach, S. Galera and K. Wien, Nucl. Instr. & Meth. in Phys. Res. B52, (1990), 121

[7] R.D. Macfarlane, C.J. McNeal and C.R. Martin, Anal. Chem., 58, 6, (1986), 1091

[8]G. Fuchs, D. Neiman, H. Poppa, Thin. Solid. Films, 207, (1992), 65.

[9]L. Bachmann, H. Hilbrand, in Basic Problems in Thin Solid Films ed. by R. Niedermayer and H. Mayer,(Physics, Vandenhoech & Ruprecht, Goettingen, 1966), p77.

[10] J.A.J. Lourens, S. Arajs, H.F. Helbig, El-Sayed A. Mehanna and L. Cheriet, Phys. Rev. B 37, (1988), 5423.

[11] B. Blanchard, H. Blanchard, J.-S. Danel and A. Ermolieff, CEA Internal Report, (1990)

[12] A. Masson, "Contributions of Cluster Physics to Material Science and Technology", ed. by J. Davenas and P.M. Rzabette (Martinus Nijhoff Publishers-Dordrech 1986) p. 295

[13] P. Mélinon, G. Fuchs, B. Cabaud, A. Hoareau, P. Jensen, V. Paillard and M. Treilleux.

J. Phys. France, 3, 1585 (1993).

[14] G. Fuchs, P. Mélinon, F.S. Aires, M. Treilleux B. Cabaud and A. Hoareau, Phys. Rev. B, 44(8), 3926 (1991)

[15] P. Mélinon, P. Jensen, J.X. Hu, A. Hoareau, B. Cabaud, M. Treilleux and D. Guillot, Phys. Rev. B44 (22), 12562 (1991)

[16] K. Sattler, J. Muhlbach and E. Recknagel, Phys. Rev. Lett., 45, 821, (1980)

[17] D. Rayane, P. Mélinon, B. Tribollet, B. Cabaud, A. Hoareau and M. Broyer, J. Chem. Phys., 91, 3100 (1989)

[18] A. Oladipo, M. Fallavier and J-P. Thomas, Int. J. of Mass Spec. and Ion Proc., 105 (1991), 119

[19] H. Allali, B. Nsouli and J-P. Thomas, Int. J. of Mass Spec. and Ion Proc., 127 (1993) 111

[20] H. Allali, B. Nsouli, J-P. Thomas, W. Szimczack and K. Wittmaack, to be published in Nucl. Instr. & Meth. in Phys. Res. B.1993

[21] H. Allali, Thesis, University of Lyon, (1993, unpublished).

[22] I.A. Baranov, A.S. Krivokhatskii and V.V. Obnorskii, Sov. Phys. Tech. Phys. 26, 12, (1981) 1455

Figure Caption

Figure 1: Alpha-particles RBS spectrum of a chromium layer 1 nm thick deposited onto a quartz substrate (3 MeV, $\theta = 150°$)

Figure 2: TEM micrograph of a sample representative of a 1 nm thick chromium layer deposited onto a quartz substrate. Such samples consist of small quartz particles covered with chromium, collected onto a holey carbon grid from the scatching of the chromium-covered side of the crystal.

Figure 3: Sketch of the TOF spectrometer experimental setup using the "start electron" technique (see text).- SBD: Surface barrier detector, MCP: Multi-channel-Plate, CFD: Constant fraction Discriminator.

Figure 4 : Mass spectra of negative ions emitted from (a) a quartz substrate, (b) a 1 nm thick Cr layer onto quartz, (c) a 0.5 nm thick SiO_x layer deposited on a chromium substrate and (d) a 1 nm thick SiO_x layer on the same substrate.

Figure 5 : Mass spectra of negative ions emitted from a Sb layer (1.6 nm thick) deposited on a Si substrate.

Figure 6 : Variation of the secondary ion yields characteristic of the layer and the substrate as a function of the layer thickness: (a) for the system Cr/quartz, (b) for the system SiO_x/Cr
The corresponding anions are indicated as well as the sample origin (different batches underlined).

Figure 7: Relative variation of theY/Y_0 yield of various substrates covered with a SiOx layer of increasing thickness. Y_0 is the yield of the ion indicated in the graph for the uncovered

substrate. Inserted is the relative yield values obtained for the 0.5 nm thickness and plotted as a function of the mass of the cluster emitted from the indicated substrate.

Figure 8: Evolution of the coverage rate (Θ) versus the LECBD film thickness. The experimental points (curve (c)) are compared with two models : curve (a) presents the theoretical coverage rate evolution when the overlapping events are neglected, while curve (b) considers these events.

Figure 9 : Variation of the yield of the ions SbO_2^- and $Sb_2O_4^-$, emitted from LECBD Sb film, as a function of coverage rate Θ.

RBS (A°)	5.0	10.6	8.6	14.5	24	37.5	42	101
Quartz crystal oscillator (A°)	5	10	10	15	25	35	50	100

Table 1

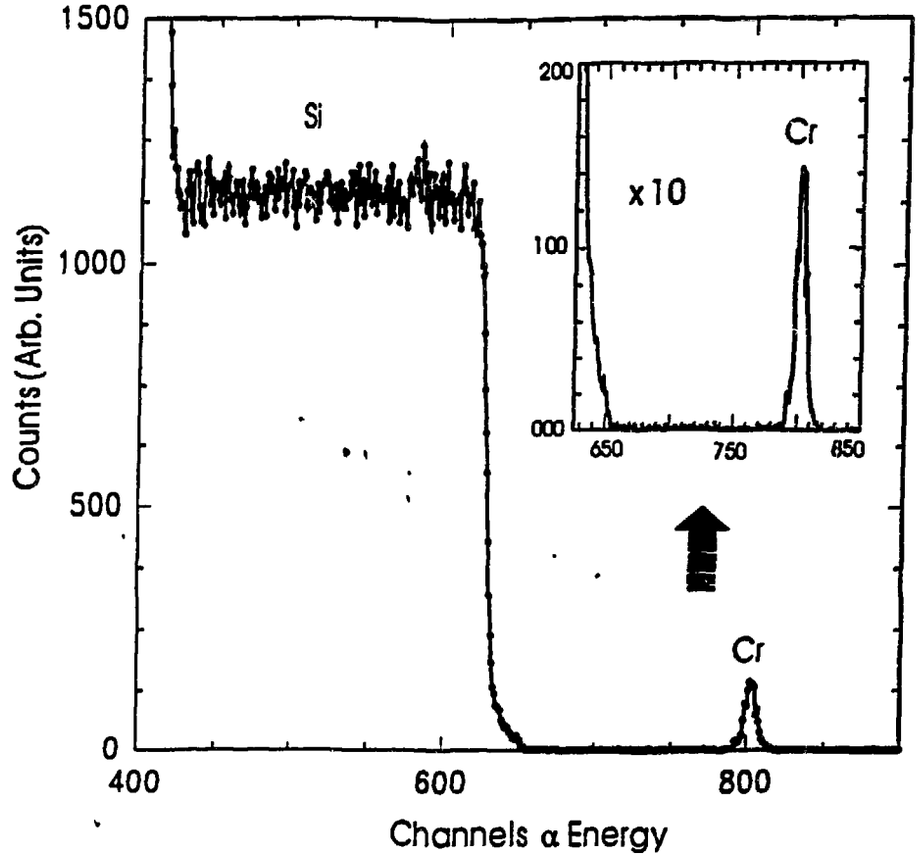
1500
1000
500
0
Counts (Arb. Units)
Si
Cr
400
600
800
Channels α Energy
200
100
000
x10
650
750
850
Cr

Fig. 1

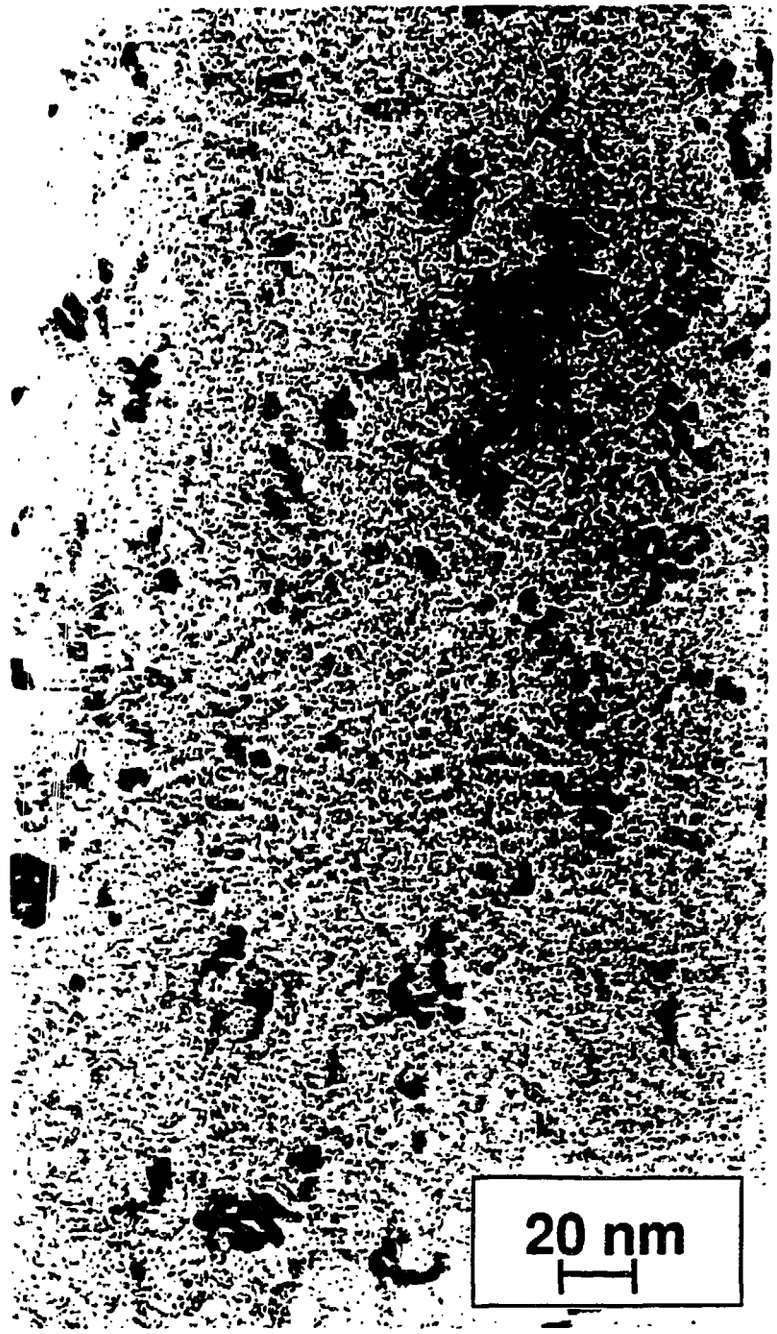
20 nm

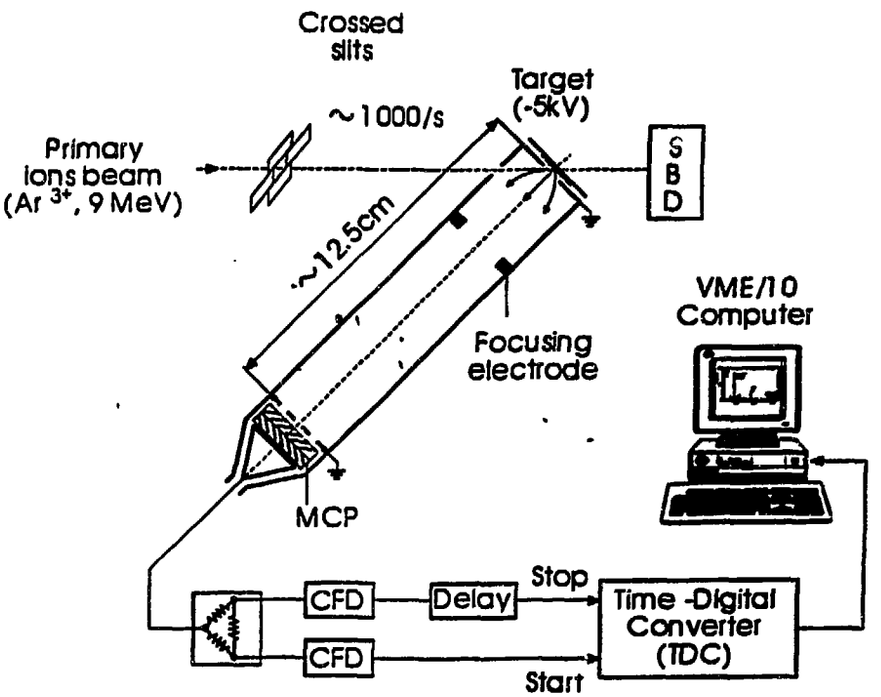

Experimental setup start electrons

Fig. 3

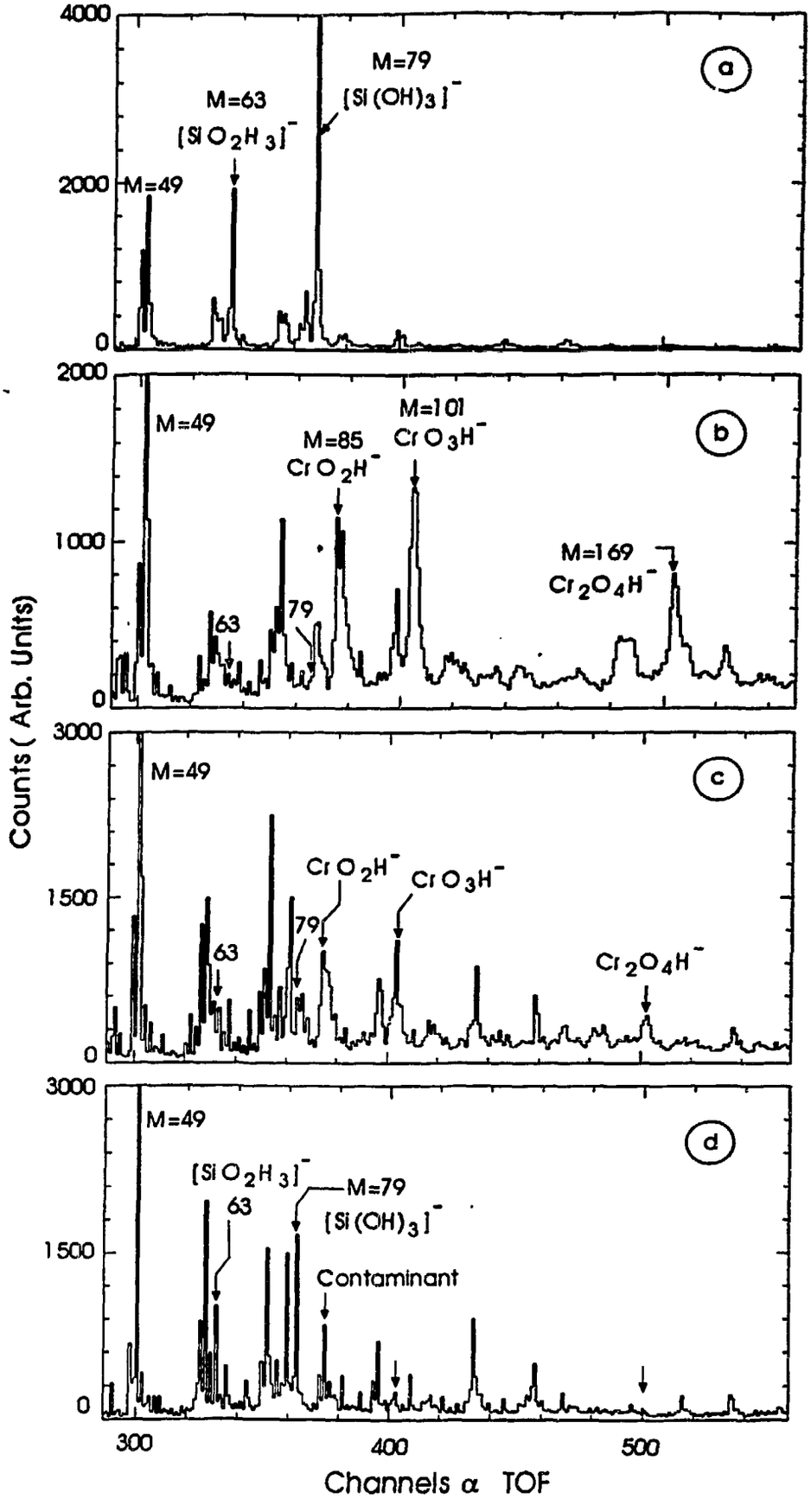
4000
2000
0
M=79
[Si(OH)3]-
M=63
[SiO2H3]-
M=49
a
2000
1000
0
M=49
M=85
CrO2H-
M=101
CrO3H-
M=169
Cr2O4H-
63
79
b
3000
1500
0
M=49
CrO2H-
CrO3H-
79
63
Cr2O4H-
c
3000
1500
0
M=49
[SiO2H3]-
63
M=79
[Si(OH)3]-
Contaminant
d
Counts (Arb. Units)
300
400
500
Channels α TOF

Fig. 4

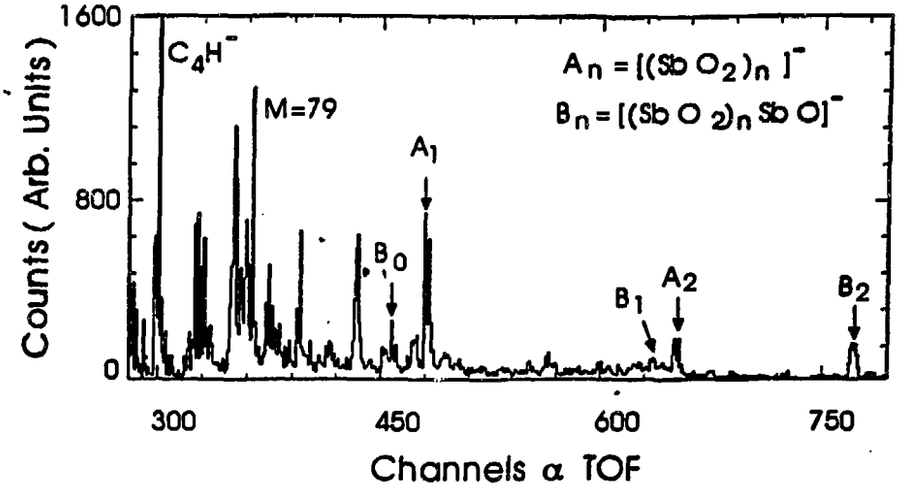
1600
800
0
Counts (Arb. Units)
C_4H^-
M=79
A_1
B_0
B_1
A_2
B_2
$A_n = [(Sb\ O_2)_n]^-$
$B_n = [(Sb\ O_2)_n\ Sb\ O]^-$
300
450
600
750
Channels α TOF

FIG. 5

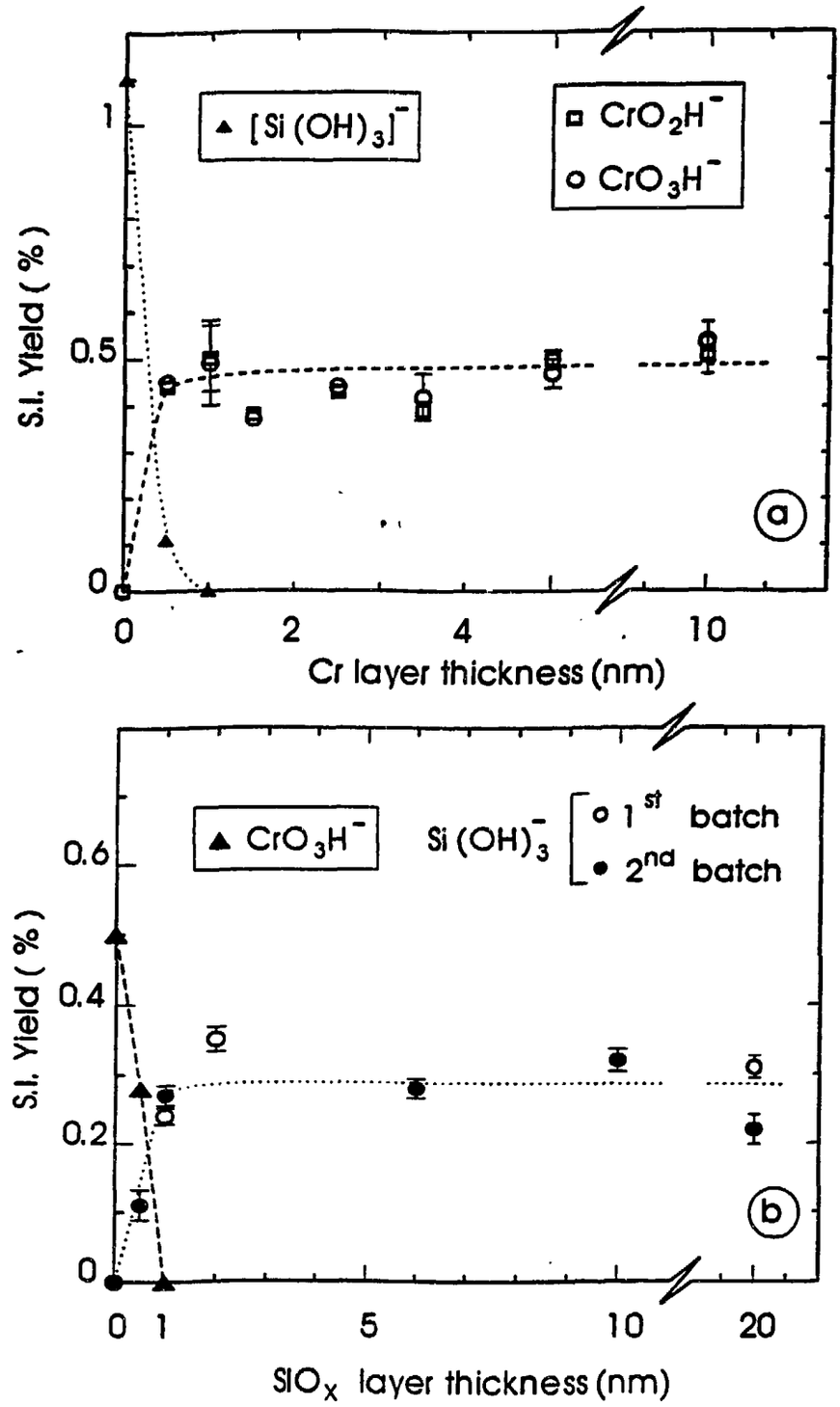
▲ [Si (OH)3]⁻
□ CrO2H⁻
○ CrO3H⁻
S.I. Yield (%)
1
0.5
0
0
2
4
10
Cr layer thickness (nm)
a
▲ CrO3H⁻
Si (OH)3⁻
○ 1st batch
● 2nd batch
S.I. Yield (%)
0.6
0.4
0.2
0
0 1
5
10
20
SiOx layer thickness (nm)
b

Fig. 6

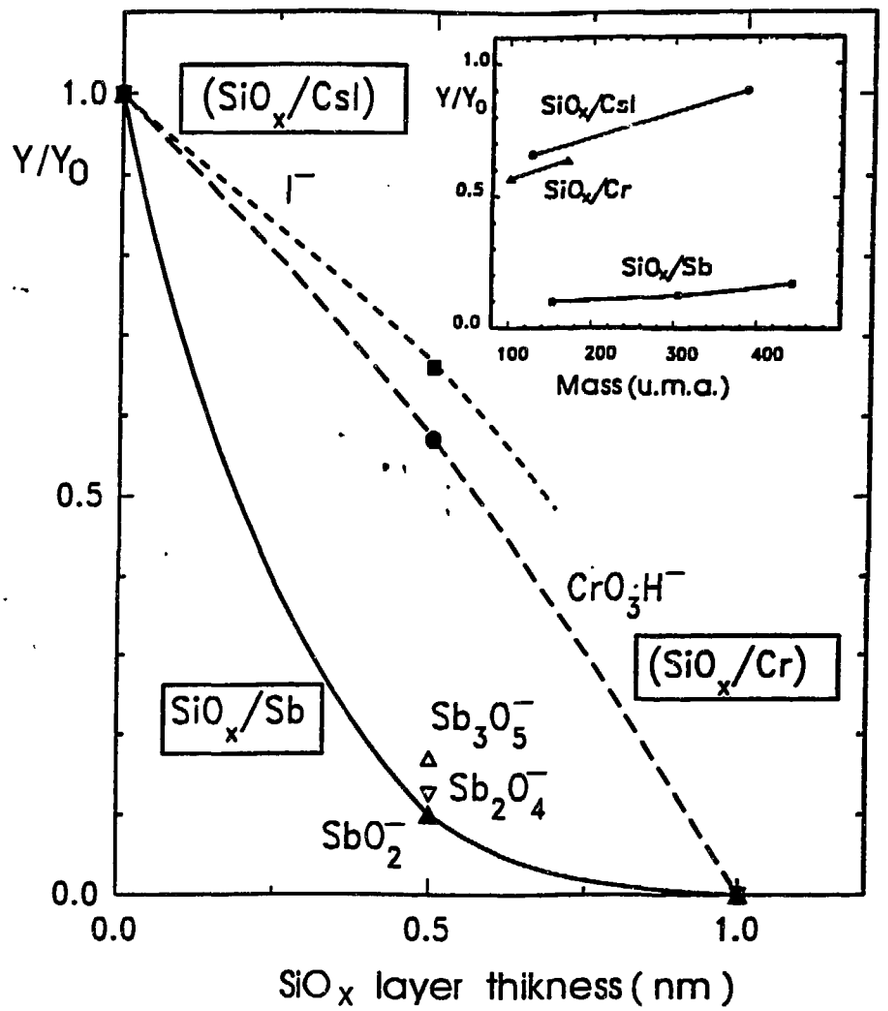
1.0
0.5
0.0
Y/Y0
(SiOx/CsI)
I−
CrO3H−
(SiOx/Cr)
SiOx/Sb
Sb3O5−
Sb2O4−
SbO2−
0.0
0.5
1.0
SiOx layer thikness (nm)
Y/Y0
SiOx/CsI
SiOx/Cr
SiOx/Sb
100
200
300
400
Mass (u.m.a.)

Fig. 7

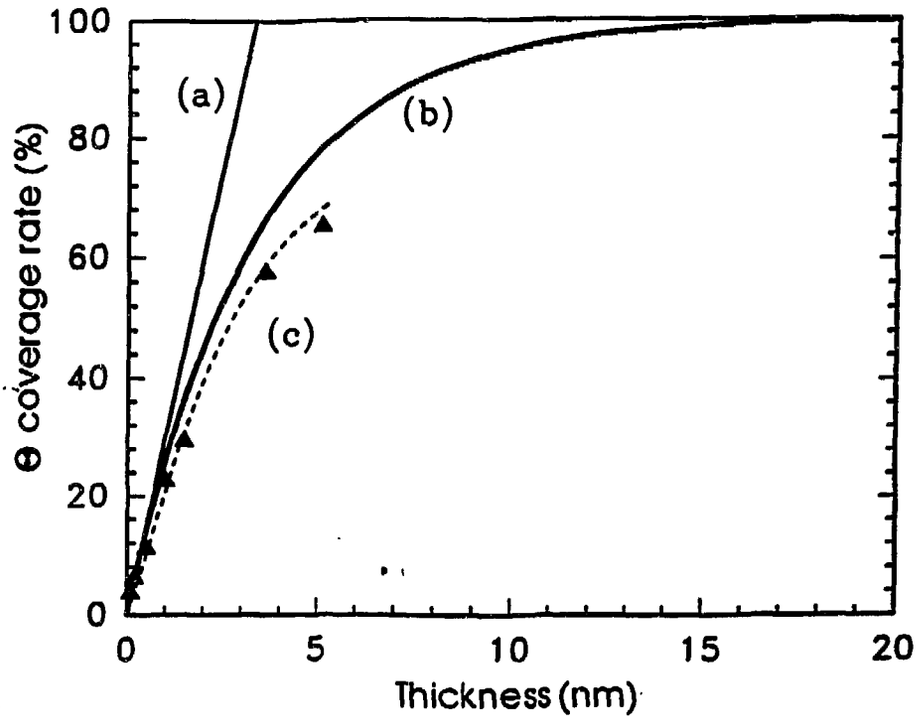
100
80
60
40
20
0
Θ coverage rate (%)
(a)
(b)
(c)
0
5
10
15
20
Thickness (nm)

Fig. 8

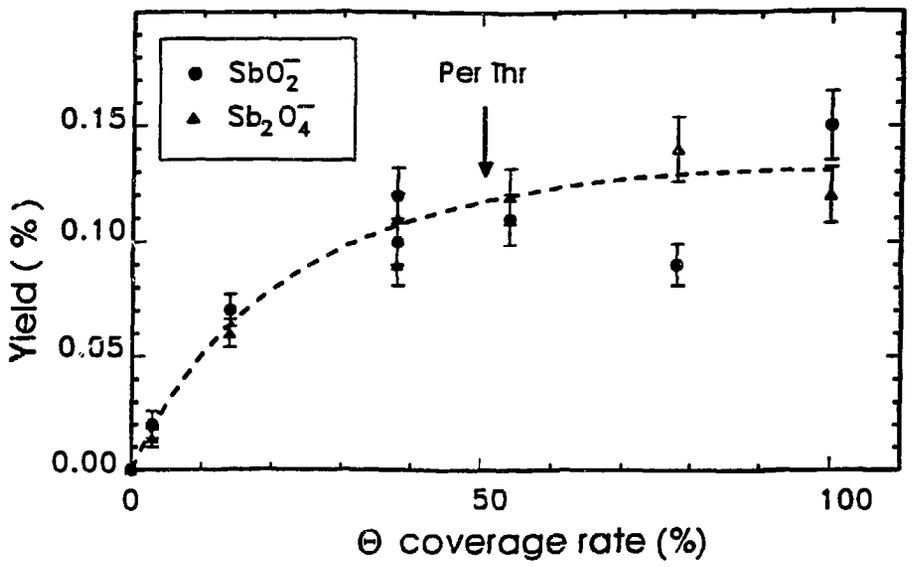
SbO2−
Sb2O4−
Per Thr
0.15
0.10
0.05
0.00
Yield (%)
0
50
100
Θ coverage rate (%)

Fig. 9